Journal of Sound and Vibration ▮ (▮▮▮▮) ▮▮▮–▮▮▮

Contents lists available at ScienceDirect

Journal of Sound and Vibration

journal homepage: www.elsevier.com/locate/jsvi

Optimal integral force feedback for active vibration control

Yik R. Teo*, Andrew J. Fleming

Precision Mechatronics Lab, School of Electrical Engineering and Computer Science, Faculty of Engineering and Built Environment, The University of Newcastle, Callaghan, New South Wales 2308, Australia

ARTICLE INFO

Article history:
Received 29 October 2014
Received in revised form
1 May 2015
Accepted 27 June 2015
Handling Editor: J. Lam

ABSTRACT

This paper proposes an improvement to Integral Force Feedback (IFF), which is a popular method for active vibration control of structures and mechanical systems. Benefits of IFF include robustness, guaranteed stability and simplicity. However, the maximum damping performance is dependent on the stiffness of the system; hence, some systems cannot be adequately controlled. In this paper, an improvement to the classical force feedback control scheme is proposed. The improved method achieves arbitrary damping for any mechanical system by introducing a feed-through term. The proposed improvement is experimentally demonstrated by actively damping an objective lens assembly for a high-speed confocal microscope.

1. Introduction

The presence of undesirable vibrations is known to degrade the performance of structural and mechanical systems that may lead to system failures and malfunctions [1]. Vibrations appear due to the unwanted excitation of system resonances. A common method for reducing vibration is to artificially increase the viscous damping in the system. Damping control can be classified into passive or active. Examples of traditional passive approaches include viscoelastic damping and tuned-mass absorbers [2]. These approaches are commonly integrated into the structural or mechanical design and eliminate the need of additional controlled hardware and sensors. However, passive damping methods can be sensitive to changes in resonance frequencies, may be bulky, and may not perform well at low frequencies. On the other hand, active damping control has the potential to overcome the performance limitations of passive damping methods [3,4]. Active control typically requires the integration of sensors and a feedback control system to artificially increase the damping ratio of a system.

Active damping control can be found in scientific and industrial applications where the speed and accuracy are key performance criteria, for example, scanning probe microscopy [5–8], nano-fabrication [9,10], precision optics [11,12], robotics [13], medical [14] and aerospace systems [15]. In addition, active damping control can also be found in defence applications where the system lifetime is important [16]. A number of techniques for damping control have been demonstrated successfully in the literature, these include Positive Position Feedback (PPF) [17], polynomial based control [18], acceleration feedback [19], shunt control [20,21], resonant control [22], Force Feedback [23–26], and Integral Resonance Control (IRC) [27,28]. Among these techniques, PPF controllers, velocity feedback controllers, force feedback controllers, and IRC controllers have been shown to guarantee stability when the plant is strictly negative imaginary [29]. Controllers with automatic synthesis have also been successfully applied to vibration control applications. Examples include robust

* Principal corresponding author.
E-mail addresses: yik.teo@newcastle.edu.au (Y.R. Teo), andrew.fleming@newcastle.edu.au (A.J. Fleming).

http://dx.doi.org/10.1016/j.jsv.2015.06.046
0022-460X/

$\mathcal{H}_\infty$ controllers [30–32] and LMI based controllers [33]. However, such methods are rarely used in practice because of their implementation complexity.

In Refs. [23–26] Integral Force Feedback (IFF) is described for vibration control. This technique utilizes a force sensor and an integral controller to directly augment the damping of a mechanical system. The major advantages of IFF are the simplicity of the controller, guaranteed stability, excellent performance and robustness to variation of resonance frequency. However, the maximum damping achievable with IFF is a function of the system properties, in particular the system's stiffness relative to the actuator stiffness. This means that some systems can be critically damped using IFF while other systems exhibit insufficient damping.

In this work, an improvement to integral force feedback is described which allows an arbitrary damping ratio to be achieved for a mechanical system. The modification amounts to replacing the integral controller with a first-order low-pass filter. Although the additional complexity is negligible, the damping performance is significantly improved. This result allows integral force feedback control to be applied to systems that were not previously suited.

2. Classical integral force feedback (CIFF)

Integral force feedback control has been widely employed for augmenting the damping of flexible structures. The feedback law is simple to implement and under common circumstances provides excellent damping performance with guaranteed stability. Fig. 1 illustrates a structure G equipped with a piezoelectric actuator that produces a force F_a with internal stiffness K_a. A force sensor is collocated with the piezoelectric actuator and measures the axial force F_s acting on the system G. The variable d represents the mechanical displacement.

The classical integral force feedback controller has a block diagram representation illustrated in Fig. 2. The transfer function between the unconstrained piezo expansion δ to the sensor force F_s is adapted from [23]

$$G_{F_s\delta}(s) = \frac{F_s}{\delta} = K_a\left\{1 - \sum_{i=1}^{n} \frac{v_i}{1+s^2/\omega_i^2}\right\}, \tag{1}$$

where ω_i is the natural frequency of the system and v_i is the fraction of modal strain energy for the ith mode. The modal zeros z_i are given as

$$z_i^2 = \omega_i^2(1-v_i). \tag{2}$$

The integral force feedback controller is

$$C_{d1}(s) = \frac{K_{d1}}{K_a s}, \tag{3}$$

where K_{d1} is the gain of controller. The maximum modal damping is [23]

$$\zeta_i^{\max} = \frac{\omega_i - z_i}{2\omega_i}, \tag{4}$$

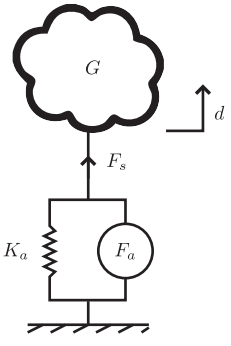

Fig. 1. Structure G with a piezoelectric transducer.

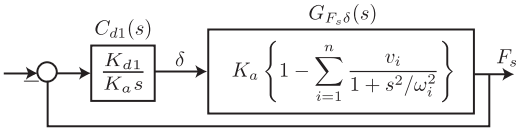

Fig. 2. Block diagram representation of Classical Integral Force Feedback.

Please cite this article as: Y.R. Teo, & A.J. Fleming, Optimal integral force feedback for active vibration control, *Journal of Sound and Vibration* (2015), http://dx.doi.org/10.1016/j.jsv.2015.06.046

and the corresponding controller gain is

$$K_{d1} = \omega_i \sqrt{\frac{\omega_i}{z_i}}. \tag{5}$$

The proofs of (4) and (5) are given in Appendix A. The root locus plot corresponding to CIFF is shown in Fig. 3(a). The main limitation of the classical method is that the maximum modal damping (4) depends on the distance between the system poles ω_i and zeros z_i. If the distance between the pole and zero is small, the maximum modal damping achievable with CIFF is reduced.

3. Optimal integral force feedback (OIFF)

This paper proposes an improvement of the classical integral force feedback methodology. A new feed-through term β is introduced into the system as shown in Fig. 4(a). The new system in Fig. 4(a) is cast into the CIFF structure via a change of variable. This allows a straightforward comparison between the CIFF and OIFF systems and to make use of previous results reported for CIFF. In particular, the expressions for maximum modal damping (4) and controller gain (5). This is done by equating the systems in Fig. 4(a) and (b), that is

$$\begin{aligned} K_a\left\{1-\sum_{i=1}^{n}\frac{v_i}{1+s^2/\omega_i^2}\right\}+\beta &= \hat{K}_a\left\{1-\sum_{i=1}^{n}\frac{\hat{v}_i}{1+s^2/\omega_i^2}\right\}, \\ K_a+\beta-\sum_{i=1}^{n}\frac{K_a v_i}{1+s^2/\omega_i^2} &= \hat{K}_a-\sum_{i=1}^{n}\frac{\hat{K}_a\hat{v}_i}{1+s^2/\omega_i^2}. \end{aligned} \tag{6}$$

From (6) we obtain the new expressions via a change of variable

$$\hat{K}_a = K_a+\beta, \tag{7}$$

and

$$\hat{v}_i = \frac{K_a v_i}{\hat{K}_a} = \frac{K_a v_i}{K_a+\beta}. \tag{8}$$

Note that the change of variables (7) and (8) is not unique, other options are possible.

The transfer function from $\hat{\delta}$ to $\hat{F}_s$ is

$$\hat{G}_{F_s\delta}(s) = \hat{K}_a\left\{1-\sum_{i=1}^{n}\frac{\hat{v}_i}{1+s^2/\omega_i^2}\right\}. \tag{9}$$

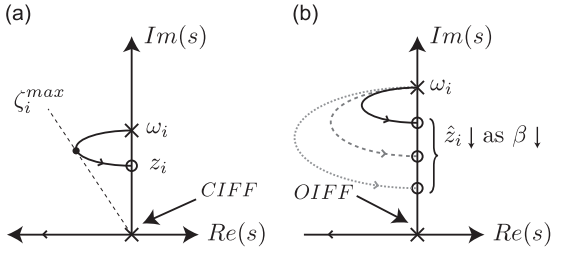

Fig. 3. Typical root locus plots. (a) Classical method. (b) Optimal method.

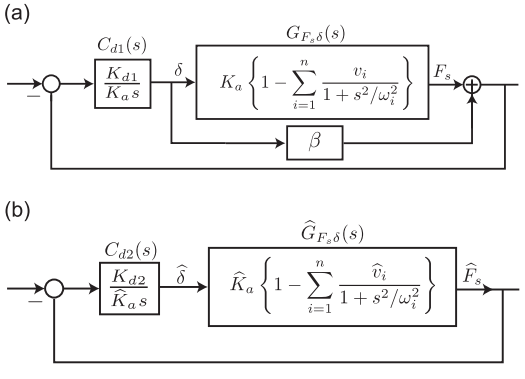

Fig. 4. Block diagram representations of Optimal Integral Force Feedback. (a) With new feed-through term β. (b) Equivalent classical form.

Please cite this article as: Y.R. Teo, & A.J. Fleming, Optimal integral force feedback for active vibration control, *Journal of Sound and Vibration* (2015), http://dx.doi.org/10.1016/j.jsv.2015.06.046

The modal zeros are now a function of β

$$\hat{z}_i(\beta) = \sqrt{\omega_i^2\left(1-\frac{K_a}{K_a+\beta}v_i\right)}. \tag{10}$$

This results in an extra degree of freedom that allows the position of the zeros to be modified. As β decreases, the zeros move closer to the real axis, under the condition that $K_a(v_i-1)<\beta<0$ is satisfied. The integral force feedback controller is

$$C_{d2}(s) = \frac{K_{d2}}{\hat{K}_a s}. \tag{11}$$

The root locus plot for a typical OIFF system is shown in Fig. 3(b). Notice that the location of the zero changes with respect to β.

The new maximum modal damping is

$$\hat{\zeta}_i^{max} = \frac{\omega_i - \hat{z}_i(\beta)}{2\hat{z}_i(\beta)}, \tag{12}$$

which corresponds to the new optimal gain

$$K_{d2} = \omega_i\sqrt{\frac{\omega_i}{\hat{z}_i(\beta)}}. \tag{13}$$

The derivations of (12) and (13) are discussed in Appendix A.

On the other hand, given a desired modal damping ζ_d, the value of β required is

$$\beta = -K_a + \frac{K_a v_i(2\zeta_d+1)^2}{4\zeta_d(1+\zeta_d)}. \tag{14}$$

3.1. Comparison between integral resonance control and integral force feedback

Integral Resonance Control is a well-known damping technique that is based on displacement feedback while Integral Force Feedback is based upon force feedback [27]. Aside from the difference feedback variables, the major difference is the open-loop structure of the systems. In IRC, the open-loop transfer function is represented by [27]

$$G_{\mathrm{IRC}}(s) = \sum_{i=1}^{n}\frac{\alpha_i}{s^2+2\zeta_i\omega_i s+\omega_i^2}, \tag{15}$$

where $\alpha_i>0\forall i$ and n represents the number of modes that sufficiently describe the properties of the structure. For IFF, the open-loop transfer function is

$$G_{\mathrm{IFF}}(s) = K_a\left\{1-\sum_{i=1}^{n}\frac{v_i}{1+s^2/\omega_i^2}\right\}, \tag{16}$$

where ω_i is the natural frequency of the system and v_i is the fraction of modal strain energy for the ith mode. In classical IFF, the only control variable is the feedback gain, while in the case of IRC, the feedback gain and the feed-through variable are both variables. In the proposed method, an additional feed-through term is added to the classic IFF structure, which provides a structure similar to that found in IRC control. However, although both damping techniques introduce an additional feed-through term, the optimal values and closed-loop response are different for each case due to the different open-loop systems.

4. Case study

In this section, the performance of CIFF and OIFF is demonstrated on a simple mechanical system.

4.1. Mechanical dynamics and system properties

The mechanics of a second-order system are illustrated in Fig. 5 with parameters listed in Table 1. The equation of motion for this system is

$$M_p\ddot{d}+c_f\dot{d}+(K_a+k_f)d = F_a, \tag{17}$$

where M_p is the mass of the platform and the stiffness and damping coefficient of the flexures are denoted by k_f and c_f respectively. The force of the actuator is F_a and the stiffness is K_a. A force sensor is collocated with the actuator and measures the load force F_s. The configuration of the system is such that the actuator and the flexure appear mechanically in parallel, hence, the stiffness coefficients can be grouped together,

$$k = K_a + k_f \tag{18}$$

Please cite this article as: Y.R. Teo, & A.J. Fleming, Optimal integral force feedback for active vibration control, *Journal of Sound and Vibration* (2015), http://dx.doi.org/10.1016/j.jsv.2015.06.046

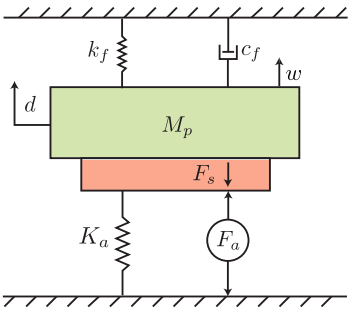

Fig. 5. Mechanical diagram of a second-order mechanical system where F_s is the measured force acting between the actuator and the mass in the vertical direction.

Table 1
Parameters of a simple mechanical system.

Parameter	Variable	Value
Mass	M_p	250 g
Flexure stiffness	k_f	300 N/μm
Actuator stiffness	K_a	100 N/μm
Flexure damping	c_f	10 N/m s^{-1}

This simplifies the equation of motion (17) to

$$M_p\ddot{d}+c_f\dot{d}+k=F_a. \tag{19}$$

The transfer function from actuator force F_a to the displacement of the mass d is

$$G_{dF_a}(s)=\frac{d}{F_a}=\frac{1}{M_ps^2+c_fs+k} \tag{20}$$

The sensor force F_s can be written as

$$\begin{aligned} F_s &= F_a-dK_a,\\ &= F_a-K_aF_aG_{dF_a}(s),\\ &= F_a\left(1-K_aG_{dF_a}(s)\right). \end{aligned} \tag{21}$$

The transfer function between the applied force F_a and measured force F_s is found by rearranging (21).

$$G_{F_sF_a}(s)=\frac{F_s}{F_a}=1-K_aG_{dF_a}(s). \tag{22}$$

The force developed by the actuator F_a is

$$F_a=K_a\delta. \tag{23}$$

Recall that δ is the unconstrained piezo expansion.

Substituting (23) into (22), we obtain the transfer function from the unconstrained piezo expansion δ to the force of the sensor F_s

$$\begin{aligned} G_{F_s\delta} &= \frac{F_s}{\delta},\\ &= K_a\frac{F_s}{F_a},\\ &= K_a\left(1-K_aG_{dF_a}(s)\right). \end{aligned} \tag{24}$$

A valid assumption is that the effect of the damping in the flexure c_f is small and thus negligible. Hence, equating (1) and (24) results in an expression for v_i and ω_i

$$\begin{aligned} K_a\left\{1-\sum_{i=0}^{n}\frac{v_i}{1+s^2/\omega_i^2}\right\} &= K_a\left(1-K_aG_{dF_a}(s)\right)\\ &= K_a\left(1-\frac{K_a}{M_ps^2+k}\right) \end{aligned}$$

Please cite this article as: Y.R. Teo, & A.J. Fleming, Optimal integral force feedback for active vibration control, *Journal of Sound and Vibration* (2015), http://dx.doi.org/10.1016/j.jsv.2015.06.046

$$= K_a\left(1 - \frac{K_a/k}{s^2/\frac{k}{M_p}+1}\right) \tag{25}$$

where

$$v_i = \frac{K_a}{k}, \quad \omega_i^2 = \frac{k}{M_p}. \tag{26}$$

The frequency of the open-loop poles of (22) is

$$\omega_1 = \sqrt{\frac{k}{M_p}} = \sqrt{\frac{k_a + k_f}{M_p}}. \tag{27}$$

The corresponding open-loop zeros are

$$\begin{aligned} z_1 &= \sqrt{\omega_i^2(1-v_i)}, \\ &= \sqrt{\frac{K_a + k_f}{M_p}\left(1 - \frac{K_a}{k}\right)}, \\ &= \sqrt{\frac{k_f}{M_p}}. \end{aligned} \tag{28}$$

which for the system are $\omega_1 = 6.4$ kHz and $z_1 = 5.5$ kHz.

4.2. Control design

4.2.1. Classical integral force feedback

The open-loop frequency response of $G_{F_sF_a}(s)$ is shown in Fig. 6. A key observation is that its phase response lies between 0 and 180°. Fig. 7 shows a general property of flexible structures with inputs and outputs proportional to the applied and measured forces. The integral controller (3) has a constant phase lag of 90° so the loop-gain of the system lies between –90° and 90°. As a result, the closed-loop system has an infinite gain margin and a phase margin of 90°.

The optimal gain and the maximum damping ratio for the example system using CIFF is $K_{d1} = 4.3 \times 10^4$ and $\zeta_1^{max} = 0.077$ respectively. These values can be validated by the numerical root-locus plot shown in Fig. 9. The numerically obtained optimal gain is 4.57×10^4 and the corresponding damping ratio is 0.077. This correlates closely with the predicted values which supports the accuracy of the assumptions made in deriving the optimal gain.

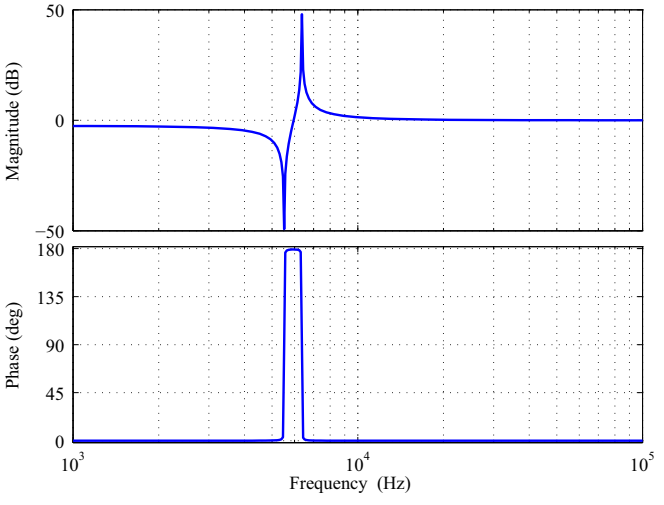

Fig. 6. Frequency response of $G_{F_sF_a}(s)$.

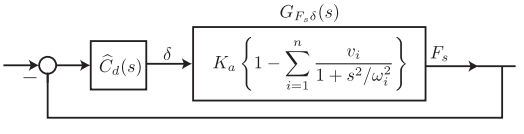

Fig. 7. Block diagram of the mechanical system using OIFF.

Please cite this article as: Y.R. Teo, & A.J. Fleming, Optimal integral force feedback for active vibration control, *Journal of Sound and Vibration* (2015), http://dx.doi.org/10.1016/j.jsv.2015.06.046

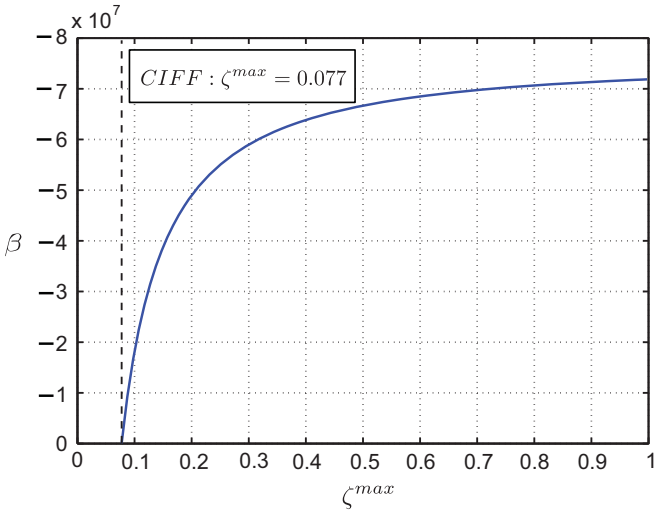

Fig. 8. The relationship between β and ζ for OIFF.

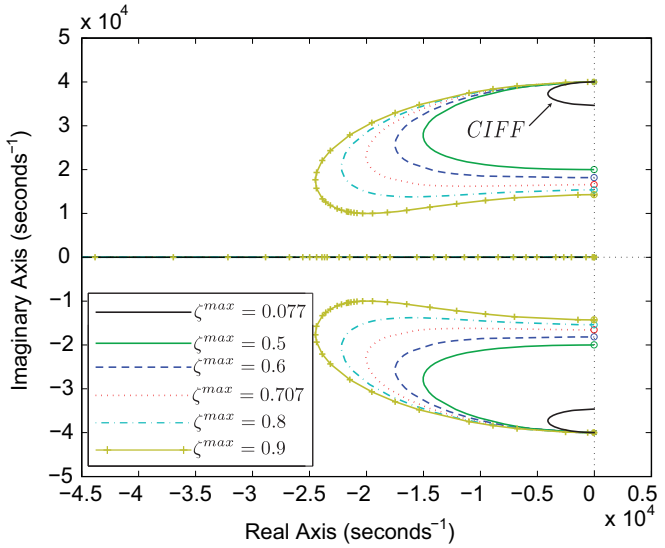

Fig. 9. Root locus comparison between CIFF and OIFF.

Table 2
Comparison between analytic and numerically obtained damping ratio and feedback gain.

β	Analytic		Numerical	
	$\hat{\zeta}^{\max}$	K_{d2}	$\hat{\zeta}^{\max}$	K_{d2}
-6.67×10^7	0.500	5.65×10^4	0.501	5.57×10^4
-6.85×10^7	0.600	5.93×10^4	0.601	5.94×10^4
-6.98×10^7	0.707	6.21×10^4	0.708	6.23×10^4
-7.07×10^7	0.800	6.45×10^4	0.801	6.49×10^4
-7.13×10^7	0.900	6.69×10^4	0.902	6.70×10^4

4.2.2. *Optimal integral force feedback*

The CIFF method can be extended to include the feed-through term β as illustrated in Fig. 4(a). For practical implementation, the equivalent controller $\hat{C}_d(s)$ presented to the plant, i.e. the transfer function from F_s to δ, is found as

$$\hat{C}_d(s)=\frac{C_{d2}(s)}{1+C_{d2}(s)\beta}. \tag{29}$$

Please cite this article as: Y.R. Teo, & A.J. Fleming, Optimal integral force feedback for active vibration control, *Journal of Sound and Vibration* (2015), http://dx.doi.org/10.1016/j.jsv.2015.06.046

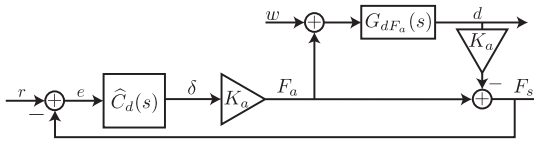

Fig. 10. Block diagram of the CIFF system for analysis.

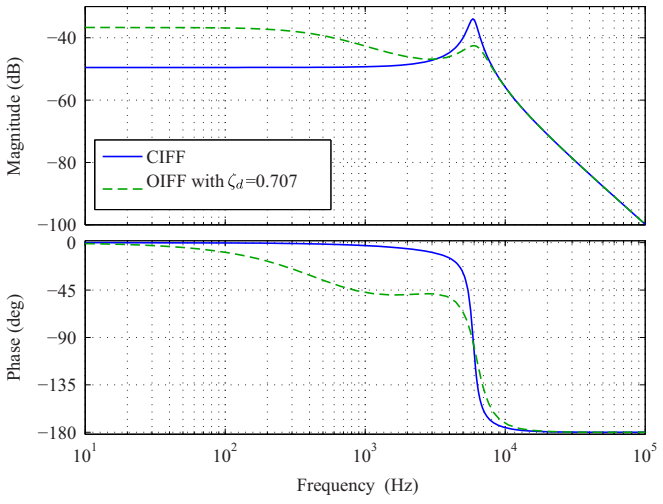

Fig. 11. Frequency response of $G_{d\omega}(s)$, where d is scaled to μm.

Fig. 12. Queensgate OSM-Z-100B objective lens positioner and Olympus 100 x objective lens.

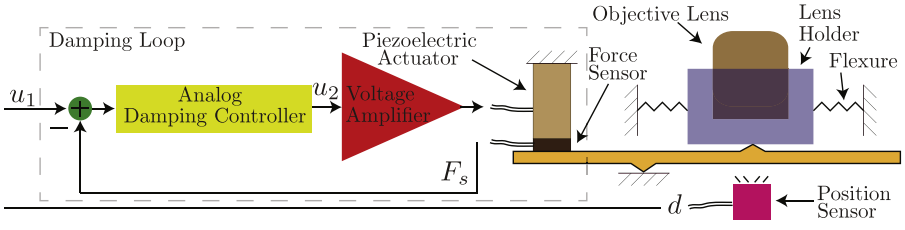

Fig. 13. Block diagram of the experimental set-up.

The additional "feed-through" term β is effectively added into the controller. Hence, no physical modification of piezoelectric actuator or mechanical system is required.

The relationship between β and ζ described in (14) for the case study is plotted in Fig. 8. The maximum modal damping with CIFF is 0.077; however, with OIFF, the maximum modal damping ranges from 0.077 to 1 with different values of β.

Please cite this article as: Y.R. Teo, & A.J. Fleming, Optimal integral force feedback for active vibration control, *Journal of Sound and Vibration* (2015), http://dx.doi.org/10.1016/j.jsv.2015.06.046

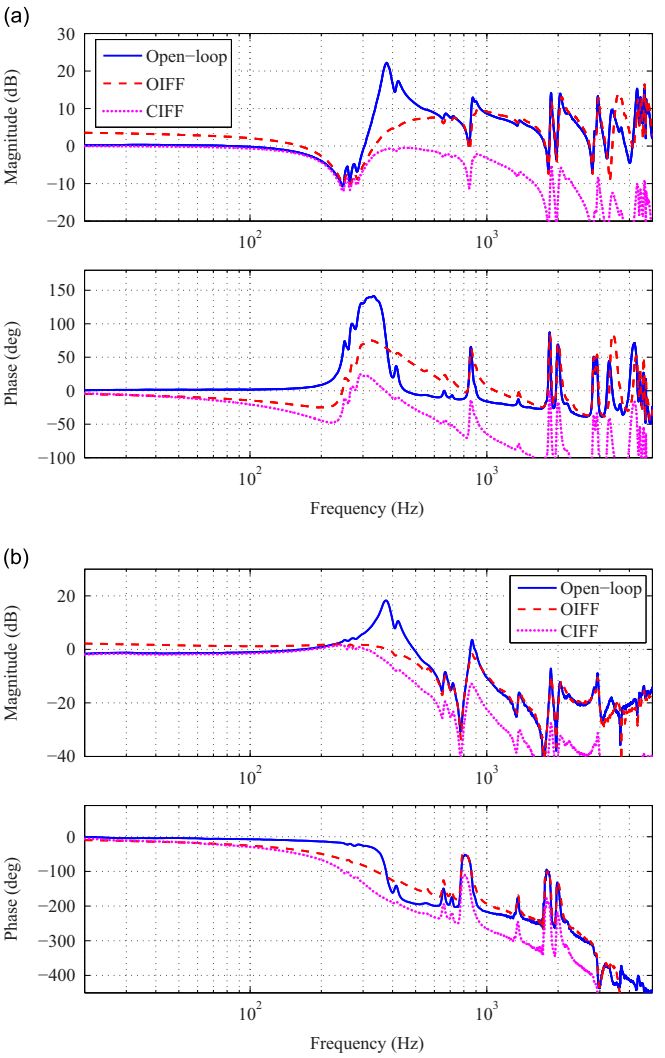

Fig. 14. Experimental results: Open and closed-loop frequency responses using CIFF and OIFF. (a) Open-loop frequency response measured from the input of the voltage amplifier u_2 to the output of the force sensor F_s and closed-loop frequency response measured from u_1 to the output of the force sensor F_s for CIFF and OIFF. (b) Open-loop frequency response measured from the input of the voltage amplifier u_2 to the output of the position sensor d and closed-loop frequency response measured from u_1 to the output of the position sensor d for CIFF and OIFF.

The root locus of the system is shown in Fig. 9. The optimal feedback gain, maximum damping ratio and corresponding value of β are given in Table 2. These values are validated by the numerical root-locus plot in Fig. 9 which is also given in Table 2. These values correlate closely with the predicted values which support the accuracy of the assumptions made in deriving the optimal gain. The closed-loop transfer function between the reference r to the sensor force F_s is

$$G_{F_s r}(s) = \frac{F_s}{r} = \frac{\hat{C}_d G_{F_s\delta}}{1 + \hat{C}_d G_{F_s\delta}}. \tag{30}$$

when $s = 0$

$$G_{F_s r}(0) = \frac{\hat{C}_d G_{F_s\delta}(0)}{1 + \hat{C}_d G_{F_s\delta}(0)} = \frac{G_{F_s\delta}(0)}{G_{F_s\delta}(0) + \beta}. \tag{31}$$

This shows that the DC gain of the closed-loop increases as β is decreased. Recall that the maximum damping ratio of the closed-loop system increases as β is decreased.

Please cite this article as: Y.R. Teo, & A.J. Fleming, Optimal integral force feedback for active vibration control, *Journal of Sound and Vibration* (2015), http://dx.doi.org/10.1016/j.jsv.2015.06.046

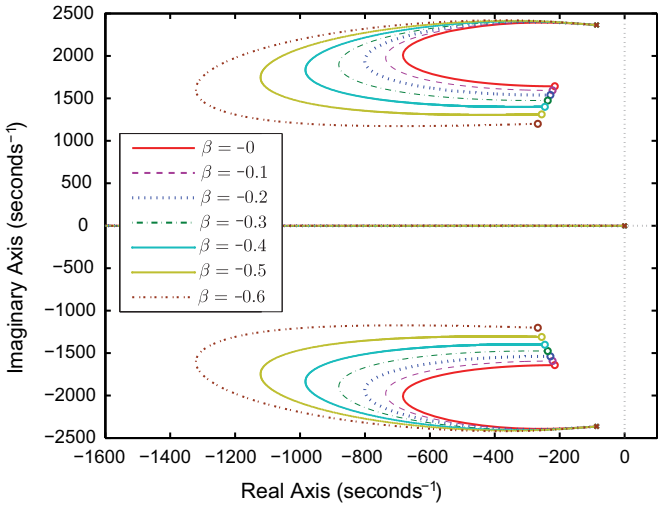

Fig. 15. Experimental results: root locus using OIFF.

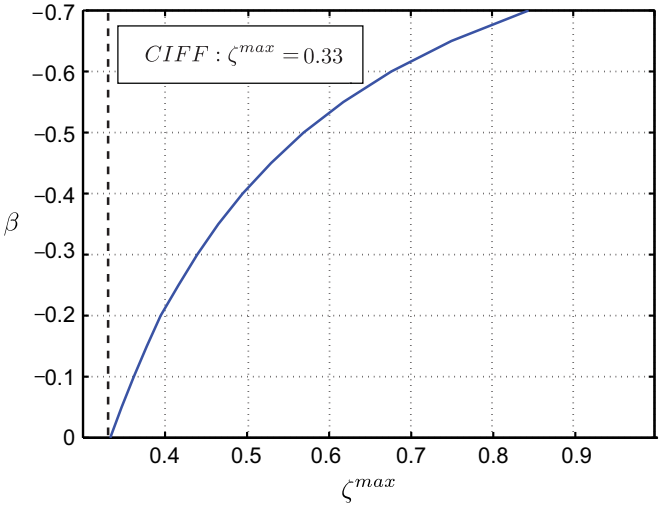

Fig. 16. Experimental relationship between ζ and β using OIFF.

Table 3
Experimental results: numerically obtained data.

β	$\hat{\zeta}^{\max}$	K_{d2}	β	$\hat{\zeta}^{\max}$	K_{d2}
0.0	0.33	1700	−0.4	0.49	2350
−0.1	0.36	1840	−0.5	0.57	2500
−0.2	0.39	2060	−0.6	0.68	2840
−0.3	0.44	2160	−0.7	0.85	3300

4.3. *Effects of external force disturbance*

We examine the effect of external force disturbances to the system. Consider the block diagram shown in Fig. 10, where an external force disturbance ω acts on the platform of the system in addition to the actuator force F_a. The transfer function from the disturbance ω to the displacement of the platform d is

$$G_{d\omega}(s) = \frac{G_{dF_a}(1+\hat{C}_d K_a)}{1+\hat{C}_d K_a(1-K_a G_{dFa})} \tag{32}$$

Fig. 11 shows the frequency response of $G_{d\omega}(s)$ for both CIFF and OIFF with $\zeta_d = 0.707$. From the frequency response, we can conclude that the improvement in damping results in a system that is more sensitive to external force disturbance.

Please cite this article as: Y.R. Teo, & A.J. Fleming, Optimal integral force feedback for active vibration control, *Journal of Sound and Vibration* (2015), http://dx.doi.org/10.1016/j.jsv.2015.06.046

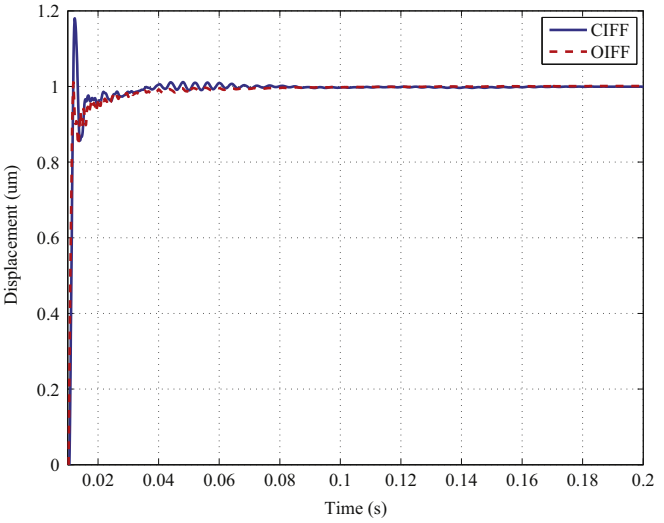

Fig. 17. Step response of the system using CIFF and OIFF with a reference of 1 μm.

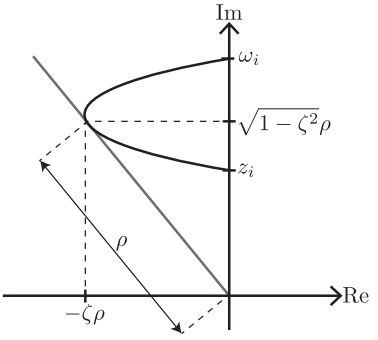

Fig. 18. Root locus plot of a system.

5. Experimental results

The experiment was conducted on a Queensgate OSM-Z-100B objective lens positioner and Olympus 100× objective lens as shown in Fig. 12. This single-axis lens positioner has a range of 100 μm and a static stiffness of 1.5 N m^{-1}. The weight of the objective lens is 88.8 g. The damping controller is implemented using analogue electronics. The block diagram of the experimental set-up is shown in Fig. 13. The open-loop frequency response of the stage was measured from the input of the voltage amplifier u_2 which is proportional to the input force F_a to the force sensor F_s and position sensor output d. The frequency responses were measured using a HP 89410A vector signal analyser with an excitation of 100 mV$_{pp}$ random noise signal.

The open-loop frequency responses are shown in Fig. 14. The open-loop resonance frequency is around 383 Hz. The frequency responses in Fig. 14 reveal an extremely high modal density. The first two modes are relative close in frequency. The root locus of the system using CIFF corresponds to $\beta = 0$ in Fig. 15. Here, the optimal gain and maximum damping ratio are numerically obtained from the root locus plot.

$$K_{d1} = 1700, \quad \zeta^{max} = 0.33 \tag{33}$$

Fig. 15 also includes the root locus plots of the system using OIFF at different values of β. The relationship between β and ζ (shown in Fig. 16) was numerically found from the root locus plot. These values are summarised in Table 3. The maximum damping ratio can be increased from 0.33 to 0.85 by adjusting the value of the feed through term β. Fig. 14 also shows the closed-loop frequency responses of the system using CIFF and OIFF with $\beta = -0.6$. The closed-loop frequency responses are measured from u_1 to the force sensor F_s and position sensor output d. The closed-loop response shows that with both method the first mode has been effectively damped. However, the damping ratio and settling time improvements cannot be directly observed from the frequency plots because of the difference in DC gain.

The most direct method for experimentally observing damping ratio and settling time is the step response of the system which is plotted in Fig. 17. The overshoot of the system with CIFF is 18 percent as compared to 1 percent for the system with OIFF. This shows the significant improvement in the system's damping. Furthermore, the 0.1 percent settling time of the

Please cite this article as: Y.R. Teo, & A.J. Fleming, Optimal integral force feedback for active vibration control, *Journal of Sound and Vibration* (2015), http://dx.doi.org/10.1016/j.jsv.2015.06.046

system with CIFF controller is 0.173 compared to 0.102 for the system with OIFF, an improvement of over 40 percent. The additional oscillation in both step responses is due to the uncontrolled higher-order dynamics of the system.

6. Conclusion

This paper describes an extension to integral force feedback damping control that allows arbitrary mechanical damping to be achieved for any mechanical system. An additional feed-through term is added to the system to provide an extra degree of freedom that can be used to arbitrarily manipulate the system zeros and maximum damping. Simulation results on a second-order system demonstrate an increase in the maximum achievable damping from 0.077 to 1 using the proposed extension. This result will allow high-performance mechanical systems to be critically damped with a first-order control law. The experimental results on a objective lens positioner demonstrate an increase in the maximum damping from 0.33 to 0.68. The closed-loop frequency responses show that the dominant first resonance mode has been attenuated by 20 dB and an improvement in the step response. Furthermore, the step response of the system with OIFF shows an significant improvement in both the overshoot and settling time as compared to the system with CIFF. Future work includes modelling the system in a negative imaginary framework to facilitate system with multiple sensors and actuators.

Acknowledgement

The authors would like to thank Prof. Andr Preumont from the Active Structures Laboratory, Universit libre de Bruxelles, Belgium for providing the solution to the maximum modal damping and controller gain for Classical Integral Force Feedback.

Appendix A. Derivation of maximum modal damping and controller gain

In a CIFF system, the closed-loop poles with open-loop system (1) and controller (3) is

$$s(s^2+\omega_i^2)+K_{d1}(s^2+z_i^2)=0, \tag{A.1}$$

where the pole position

$$s=\rho(K_{d1})(-\zeta+i\sqrt{1-\zeta^2}). \tag{A.2}$$

is a function of the integral force feedback gain K_{d1}. The expression of the maximum modal damping (4) and controller gain (5) can be found analytically from the root locus plot shown in Fig. 18. The solutions were computed using Maple, a computer algebra software. The procedures are listed below.

1. Replace (A.2) into (A.1),

$$\begin{aligned}\rho(K_{d1})\left(-\zeta+i\sqrt{-\zeta^2+1}\right)\left(\omega^2+(\rho(K_{d1}))^2\left(-\zeta+i\sqrt{-\zeta^2+1}\right)^2\right)\\ +K_{d1}\left(\omega^2+(\rho(K_{d1}))^2\left(-\zeta+i\sqrt{-\zeta^2+1}\right)^2\right)=0\end{aligned} \tag{A.3}$$

2. Separate (A.3) into real and imaginary components.

$$\begin{aligned}\text{Real: } &-4(\rho(K_{d1}))^3\zeta^3+2(\rho(K_{d1}))^2K_{d1}\zeta^2+3\zeta(\rho(K_{d1}))^3\\ &-\rho(K_{d1})\omega^2\zeta-(\rho(K_{d1}))^2K_{d1}+K_{d1}z^2\end{aligned} \tag{A.4}$$

$$\begin{aligned}\text{Imaginary: } &4(\rho(K_{d1}))^3\zeta^2\sqrt{-\zeta^2+1}-2\sqrt{-\zeta^2+1}(\rho(K_{d1}))^2K_{d1}\zeta\\ &-\sqrt{-\zeta^2+1}(\rho(K_{d1}))^3+\rho(K_{d1})\sqrt{-\zeta^2+1}\omega^2\end{aligned} \tag{A.5}$$

3. The pole position that corresponds to the maximum damping is the point when a line tangent from the origin intersects with the root locus. This can be found analytically by differentiating (A.4) and (A.5) with respect to K_{d1}, i.e. d/dK_{d1}(A.4) and d/dK_{d1}(A.5).
4. Replace the variables $\rho(K_{d1})=c_\rho$ and $d/dK_{d1}\rho(K_{d1})=c_{d\rho}$, where c_ρ and $c_{d\rho}$ are constants, into (A.4) and (A.5), d/dK_{d1}(A.4) and d/dK_{d1}(A.5).
5. Solve the four equations in Step 4 simultaneously to find solutions for the unknowns ζ, ρ, dro, K_{d1}.

Please cite this article as: Y.R. Teo, & A.J. Fleming, Optimal integral force feedback for active vibration control, *Journal of Sound and Vibration* (2015), http://dx.doi.org/10.1016/j.jsv.2015.06.046

There are eight possible solutions from Step 5, however, only one of the solutions is non-trivial and feasible. The solutions include

- Two trivial solution corresponds to $c_\rho = c_\rho$. These solutions are neglected as both the controller gain $K_{d1} = (\omega^2 + c_\rho^2)c_\rho/(c_\rho^2 + z^2)$ and $K_{d1} = -(\omega^2 + c_\rho^2)c_\rho/(c_\rho^2 + z^2)$ requires c_ρ which is still an unknown variable.
- Two solutions correspond to an imaginary valued controller gain $K_{d1} = \omega^2/\sqrt{-\omega z}, \omega z > 0$. These solutions are neglected.
- Two solutions correspond to an imaginary valued c_ρ, $\omega z > 0$. These solutions are neglected because the absolute value of a complex number has to be real valued.
- One solution corresponds to a negative valued damping ratio where $\zeta = -\omega - z/2z, \omega > z$ which is neglected.
- The remaining solution is

$$\zeta_i^{\max} = \frac{\omega_i - z_i}{2\omega_i}, \quad K_{d1} = \omega_i \sqrt{\frac{\omega_i}{z_i}}. \tag{A.6}$$

  which corresponds to the maximum damping (4) and controller gain (5) expressions.

In an OIFF system, the same proof procedure can be done to obtain the maximum modal damping (12) and controller gain (13). However, this is not required as the OIFF system can be cast into a CIFF system via a change of variables. Hence, the expressions in (4) and (5) can be re-written to incorporate the change of variables

$$\hat{\zeta}_i^{max} = \frac{\omega_i - \hat{z}_i(\beta)}{2\hat{z}_i(\beta)}, \quad K_{d2} = \omega_i \sqrt{\frac{\omega_i}{\hat{z}_i(\beta)}}. \tag{A.7}$$

References

[1] A. Preumont, *Vibration Control of Active Structures*, Kluwer Academic Publishers, 2002 http://www.springer.com/us/book/9789400720329.
[2] E.I. Rivin, *Passive vibration isolation*, ASME, 2003 https://www.asme.org/products/books/passive-vibration-isolation.
[3] D.J. Inman, *Vibration with Control*, John Wiley and Sons Ltd, Chichester, England, 2006.
[4] M. Moshrefi-Torbati, J. Forrester, A. Forrester, A. Keane, M. Brennan, S. Elliott, Novel active and passive anti-vibration mountings, *Journal of Sound and Vibration* 331 (7) (2012) 1532–1541.
[5] N. Jalili, K. Laxminarayana, A review of atomic force microscopy imaging systems: *application to molecular metrology and biological sciences*, *Mechatronics* 14 (8) (2004) 907–945.
[6] A.J. Fleming, B.J. Kenton, K.K. Leang, Bridging the gap between conventional and video-speed scanning probe microscopes, *Ultramicroscopy* 110 (9) (2010) 1205–1214, http://dx.doi.org/10.1016/j.ultramic.2010.04.016.
[7] Y.K. Yong, S.S. Aphale, S.O.R. Moheimani, Design, identification, and control of a flexure-based xy stage for fast nanoscale positioning, *IEEE Transactions on Nanotechnology* 8 (1) (2009) 46.
[8] Yin. Zhang, H. Zhao, L. Zuo, Contact dynamics of tapping mode atomic force microscopy, *Journal of Sound and Vibration* 331 (23) (2012) 5141–5152.
[9] A. Ferreira, C. Mavroidis, Virtual reality and haptics for nanorobotics, *IEEE Robotics and Automation Magazine* 13 (3) (2006) 78–92.
[10] A.A. Tseng, S. Jou, A. Notargiacomo, T.P. Chen, Recent developments in tip-based nanofabrication and its roadmap, *Journal of Nanoscience and Nanotechnology* 8 (5) (2008) 2167–2186.
[11] L. Vaillon, C. Philippe, Passive and active microvibration control for very high pointing accuracy space systems, *Smart Materials and Structures* 8 (6) (1999) 719–728.
[12] A.J. Bronowicki, N.S. Abhyankar, S.F. Griffin, Active vibration control of large optical space structures, *Smart Materials and Structures* 8 (6) (1999) 740–752.
[13] J. Lin, Z. Huang, P. Huang, An active damping control of robot manipulators with oscillatory bases by singular perturbation approach, *Journal of Sound and Vibration* 304 (1–2) (2007) 345–360.
[14] M. Jaensch, M.U. Lampérth, Development of a multi-degree-of-freedom micropositioning, vibration isolation and vibration suppression system, *Smart Materials and Structures* 16 (2) (2007) 409–417.
[15] M.D. Rao, Recent applications of viscoelastic damping for noise control in automobiles and commercial airplanes, *Journal of Sound and Vibration* 262 (3) (2003) 457–474.
[16] S.y. Wu, T.L. Turner, S.A. Rizzi, Piezoelectric shunt vibration damping of an f-15 panel under high-acoustic excitation, in: SPIE's 7th Annual International Symposium on Smart Structures and Materials, International Society for Optics and Photonics, 2000, pp. 276–287.
[17] J.L. Fanson, T.K. Caughey, Positive position feedback control for large space structures, *AIAA Journal* 28 (4) (1990) 717–724.
[18] S.S. Aphale, B. Bhikkaji, S.O.R. Moheimani, Minimizing scanning errors in piezoelectric stack-actuated nanopositioning platforms, *IEEE Transactions on Nanotechnology* 7 (1) (2008) 79–90.
[19] M. Ahmadian, S.N. Mahmoodi, Modified acceleration feedback for active vibration control of aerospace structures, *Smart Materials and Structures* 19 (6) (2010) 65015–65024.
[20] A.J. Fleming, S.O.R. Moheimani, Sensorless vibration suppression and scan compensation for piezoelectric tube nanopositioners, *IEEE Transactions on Control Systems Technology* 14 (1) (2006) 33–44.
[21] A.J. Fleming, S. Behrens, S.O.R. Moheimani, Optimization and implementation of multi-mode piezoelectric shunt damping systems, *IEEE/ASME Transactions on Mechatronics* 7 (1) (2002) 87–94.
[22] H.R. Pota, S.O.R. Moheimani, M. Smith, Resonant controllers for smart structures, in: Proceedings of IEEE Conference on Decision and Control, Phoenix, Arizona, 1999, pp. 631–636.
[23] A. Preumont, B. de Marneffe, A. Deraemaeker, F. Bossens, The damping of a truss structure with a piezoelectric transducer, *Computers & Structures* 86 (3) (2008) 227–239.
[24] A. Preumont, *Mechatronics, Dynamics of Electromechanical and Piezoelectric Systems*, Springer, Dordrecht, The Netherlands, 2006.
[25] A.J. Fleming, Nanopositioning system with force feedback for high-performance tracking and vibration control, *IEEE Transactions on Mechatronics* 15 (3) (2010) 433–447.
[26] A.J. Fleming, K.K. Leang, Integrated strain and force feedback for high performance control of piezoelectric actuators, *Sensors and Actuators A* 161 (1–2) (2010) 256–265, http://dx.doi.org/10.1016/j.sna.2010.04.008.
[27] S.S. Aphale, A.J. Fleming, S.O.R. Moheimani, Integral resonant control of collocated smart structures, *IOP Smart Materials and Structures* 16 (2007) 439–446, http://dx.doi.org/10.1088/0964-1726/16/2/023.

Please cite this article as: Y.R. Teo, & A.J. Fleming, Optimal integral force feedback for active vibration control, *Journal of Sound and Vibration* (2015), http://dx.doi.org/10.1016/j.jsv.2015.06.046

[28] A.J. Fleming, S.S. Aphale, S.O.R. Moheimani, A new method for robust damping and tracking control of scanning probe microscope positioning stages, *IEEE Transactions on Nanotechnology* 9 (4) (2010) 438–448, http://dx.doi.org/10.1109/TNANO.2009.2032418.
[29] I.R. Petersen, A. Lanzon, Feedback control of negative-imaginary systems, *IEEE Control Systems* 30 (5) (2010) 54–72.
[30] Bao-Lin. Zhang, G.-Y. Tang, Active vibration h8 control of offshore steel jacket platforms using delayed feedback, *Journal of Sound and Vibration* 332 (22) (2013) 5662–5677.
[31] N. Debnath, S. Deb, A. Dutta, Frequency band-wise passive control of linear time invariant structural systems with h8 optimization, *Journal of Sound and Vibration* 332 (23) (2013) 6044–6062.
[32] Y. Cheung, W. Wong, H-infinity optimization of a variant design of the dynamic vibration absorber–revisited and new results, *Journal of Sound and Vibration* 330 (16) (2011) 3901–3912.
[33] C. Lee, S.M. Salapaka, Fast robust nanopositioning: *a linear-matrix-inequalities-based optimal control approach*, *IEEE/ASME Transactions on Mechatronics* 14 (4) (2009) 414–422.

Please cite this article as: Y.R. Teo, & A.J. Fleming, Optimal integral force feedback for active vibration control, *Journal of Sound and Vibration* (2015), http://dx.doi.org/10.1016/j.jsv.2015.06.046